Europe PMC Funders Group
Author Manuscript
Science. Author manuscript; available in PMC 2024 May 07.

Published in final edited form as:
Science. 2024 January 05; 383(6678): 101–108. doi:10.1126/science.adj3.

Molecular insights into atypical modes of β-arrestin interaction with seven transmembrane receptors

Jagannath Maharana[#1], **Fumiya K. Sano**[#2], **Parishmita Sarma**[#1], **Manish K. Yadav**[1], **Longhan Duan**[3], **Tomasz M. Stepniewski**[4], **Madhu Chaturvedi**[1], **Ashutosh Ranjan**[1], **Vinay Singh**[1], **Sayantan Saha**[1], **Gargi Mahajan**[1], **Mohamed Chami**[5], **Wataru Shihoya**[2], **Jana Selent**[4], **Ka Young Chung**[3], **Ramanuj Banerjee**[1,*], **Osamu Nureki**[2,*], **Arun K. Shukla**[1,*]

[1]Department of Biological Sciences, Indian Institute of Technology Kanpur, Kanpur, India

[2]Graduate School of Science, The University of Tokyo, Tokyo, Japan

[3]School of Pharmacy, Sungkyunkwan University, Suwon, Republic of Korea

[4]Research Program on Biomedical Informatics, Hospital del Mar Research Institute and Pompeu Fabra University, Barcelona, Spain

[5]BioEM Lab, Biozentrum, University of Basel, Basel, Switzerland

[#] These authors contributed equally to this work.

Abstract

β-arrestins (βarrs) are multifunctional proteins involved in signaling and regulation of seven transmembrane receptors (7TMRs), and their interaction is driven primarily by agonist-induced receptor activation and phosphorylation. Here, we present seven cryo–electron microscopy structures of βarrs either in the basal state, activated by the muscarinic receptor subtype 2 (M2R) through its third intracellular loop, or activated by the βarr-biased decoy D6 receptor (D6R). Combined with biochemical, cellular, and biophysical experiments, these structural snapshots allow the visualization of atypical engagement of βarrs with 7TMRs and also reveal a structural transition in the carboxyl terminus of βarr2 from a β strand to an α helix upon activation by D6R. Our study provides previously unanticipated molecular insights into the structural and functional diversity encoded in 7TMR-βarr complexes with direct implications for exploring novel therapeutic avenues.

exclusive licensee American Association for the Advancement of Science. No claim to original US government works. https://www.science.org/about/science-licenses-journal-article-reuse

[*]**Corresponding author**. ramanujb@iitk.ac.in (R.B.); nureki@bs.s.u-tokyo.ac.jp (O.N.); arshukla@iitk.ac.in (A.K.S.).

Author contributions: Conceptualization: J.M., F.K.S., P.S., J.S., K.Y.C., R.B., O.N., and A.K.S. Methodology: J.M., F.K.S., P.S., M.K.Y., L.D., T.M.S., Ma.C., A.R., V.S., S.S., G.M., Mo.C., W.S., J.S., K.Y.C., R.B., O.N., and A.K.S. Investigation: J.M., F.K.S., P.S., M.K.Y., L.D., T.M.S., Ma.C., A.R., V.S., S.S., G.M., Mo.C., W.S., J.S., K.Y.C., R.B., O.N., and A.K.S. Visualization: J.M., F.K.S., P.S., M.K.Y., L.D., T.M.S., M.C., A.R., V.S., S.S., G.M., Mo.C., W.S., J.S., K.Y.C., R.B., O.N., and A.K.S. Funding acquisition: J.S., K.Y.C., O.N., and A.K.S. Project administration: J.S., K.Y.C., O.N., and A.K.S. Supervision: J.S., K.Y.C., O.N., and A.K.S. Writing – original draft: J.M., R.B., O.N., and A.K.S. Writing – review & editing: J.M., F.K.S., P.S., M.K.Y., J.S., K.Y.C., R.B., O.N., and A.K.S.

Competing interests: The authors declare that they have no competing interests.

Europe PMC Funders Author Manuscripts
Europe PMC Funders Author Manuscripts

Europe PMC Funders Author Manuscripts

Europe PMC Funders Author Manuscripts

β-arrestins (βarrs) are multifunctional proteins that interact with and regulate a large repertoire of G protein–coupled receptors (GPCRs) at multiple levels (1–4). The interaction of GPCRs and βarrs is typically conceived to be driven primarily by agonist-induced receptor phosphorylation and receptor activation, although emerging studies have started to suggest additional contributing factors such as membrane interaction, catalytic activation, and the role of specific phospholipids (2–10). Structures of GPCR-βarr1 complexes have provided the first glimpse of high-resolution information about this interaction (11–16). However, considering the divergent sequences and phosphorylation patterns of GPCRs, the molecular mechanisms driving the broadly conserved nature of GPCR-βarr interaction and activation have been more elusive. Recent studies have shed light on phosphorylation-mediated components of GPCR-βarr binding through broadly conserved phosphorylation motifs identified in a large number of GPCRs (17–20). For example, structural and biophysical studies have proposed the framework of phosphorylation codes and modulatory sites in the GPCR C terminus as a possible mechanism governing phosphorylation-mediated βarr interaction (19, 20). Two independent structural studies identified that the presence of a P-X-P-P–type phosphorylation motif in the C terminus of a broad set of GPCRs, where *P* is a phosphorylation site, as a critical determinant of βarr interaction and activation (17, 18).

There are several GPCRs, for example the human muscarinic receptor subtype 2 (M2R), that contain a short C terminus with few potential phosphorylation sites, but they harbor phosphorylation sites primarily in their third intracellular loop (ICL3) (5, 17, 21–23). Site-directed mutagenesis and biochemical studies have shown that phosphorylation sites in the intracellular loops of some of these receptors contribute to βarr binding (24, 25). Whether these receptors engage the same binding interface with βarrs and impart similar activation features as GPCRs with phosphorylation sites on their C terminus remains unexplored in terms of direct structural visualization. Several seven transmembrane receptors (7TMRs), such as the human decoy D6 receptor (D6R), are sometimes classified as nonsignaling or nonfunctional GPCRs, as they lack functional G protein coupling. However, these proteins robustly interact with and signal through βarrs (26–29). The molecular mechanisms used by these receptors, known as atypical chemokine receptors (ACKRs) or arrestin-coupled receptors (ACRs), to bind and activate βarrs are also mostly elusive with respect to the binding interface and activation-dependent conformational changes vis-à-vis prototypical GPCRs (30–33).

Structures reveal atypical βarr binding modes to GPCRs

To visualize atypical modes of βarr recruitment, we focused our efforts on M2R, which has a short C terminus, with most of the potential phosphorylation sites localized in ICL3, and D6R, which is an intrinsically βarr-biased receptor with no detectable G protein activation despite robust βarr binding and signaling. We also determined the structure of βarr2 in the basal conformation and in complex with a phosphopeptide derived from a prototypical GPCR, the complement C3a receptor (C3aR) (Fig. 1). For M2R, we used a full-length, wildtype receptor phosphorylated in cellulo through coexpression of a membrane-tethered G protein–coupled receptor kinase 2 construct ($GRK2^{CAAX}$) and agonist-induced phosphorylation followed by incubation with purified βarr1 and Fab30 to reconstitute the complex (fig. S1, A and B). Subsequently, we attempted to determine the

Europe PMC Funders Author Manuscripts

Europe PMC Funders Author Manuscripts

structure of this complex using cryo–electron microscopy (cryo-EM). Although the receptor component was not resolved at high resolution, presumably because of inherent flexibility, we successfully determined the structure of receptor-bound βarr1 at 3.1-Å resolution with focused refinement (Fig. 1C and fig. S2). Attempting to reduce the flexibility of the receptor component in this complex, we cross-linked the preformed M2R-βarr1-Fab30 complex using on-column glutaraldehyde cross-linking (34) followed by cryo-EM data collection. The receptor exhibited flexible positioning relative to βarr1, such that we could determine the structure of only the receptor-bound βarr1 at 3.2-Å resolution (Fig. 1C and figs. S1, C and D, and S3). These structural snapshots nevertheless allowed us to identify the phosphorylated region of the ICL3 in M2R that forms the key interaction interface with βarr1 and thereby allowed us to synthesize and validate the corresponding phosphopeptide (M2Rpp) (fig. S4, A and B) and determine the structure of the M2Rpp-βarr2-Fab30 complex at 2.9-Å resolution (Fig. 1C and figs. S1, E and F, and S5).

For D6R, we have reported previously that the critical determinants of βarr recruitment are located primarily in its C terminus (27). We therefore generated a set of phosphopeptides corresponding to the phosphorylated D6R and tested their ability to activate βarrs in vitro using Fab30 reactivity or limited proteolysis as readouts (fig. S4, C to F). On the basis of these assays, we identified D6Rpp2 (referred to hereafter as D6Rpp) as activating βarrs most efficiently, and we used it to reconstitute D6Rpp-βarr1/2-Fab30 complexes (fig. S1, G and H) and determined their structures at 3.4- and 3.2-Å resolution, respectively (Fig. 1D and figs. S6 and S7). We also determined the structures of wild-type βarr2 in its basal conformation stabilized by Fab6 (Fig. 1A and figs. S1I and S8) and βarr1 in complex with a C terminus phosphopeptide of the complement C3a receptor (C3aR), a prototypical GPCR (Fig. 1B and figs. S1J and S9), as references for basal and typical active conformations. EM densities of the phosphorylated receptor domains and the key loops in βarrs in these above-mentioned structures are presented in fig. S10.

M2R-βarr1-Fab30 resembles a hanging conformation observed previously for prototypical GPCRs (11, 34) with a space between the receptor and βarr components, presumably owing to their interaction mediated primarily through the long ICL3 (~150 residues) in the M2R (Fig. 2, A to E). This space is observed in M2R complexes with both isoforms of βarrs and after receptor phosphorylation by either GRK2 or GRK6 (Fig. 2, A to D), suggesting that hanging conformations represent a major M2R-βarr population irrespective of βarr or GRK isoforms. Glutaraldehyde cross-linking appears to stabilize a more closely engaged complex, as reflected in negative-staining two-dimensional (2D) class averages (Fig. 2G), but did not improve resolution of the receptor component in cryo-EM. The structure of M2R-bound βarr1 revealed a phosphorylated stretch of ICL3 in the receptor that harbors the residues from E305 to G313 with four phosphorylation sites (Thr^{307}, Ser^{309}, Thr^{310}, and Ser^{311}) and docks on the N-domain of βarr1 (Fig. 2, F and H). M2Rpp derived from the ICL3 sequence visualized in M2R-bound βarr1 structure binds to an analogous interface on βarr2 (Fig. 2, I and J). The βarr1 and βarr2 in these structures exhibit an interdomain rotation of ~18° and 23°, respectively (Fig. 2, F, H, and J); disruption of the three-element and polar-core network (figs. S11, A to D, and S24); and reorientation of the critical loops compared with the basal conformation (fig. S11E). The phosphate groups in the M2R-ICL3 stretch resolved in these structures are organized in a P-X-P-P pattern, where *P* is a phosphorylation

Europe PMC Funders Author Manuscripts

Europe PMC Funders Author Manuscripts

site, and are engaged in ionic interactions with conserved Lys and Arg residues in βarrs organized in a K-R-K–type pattern involving R7/R8, K10/K11, K11/K12, R25/R26, K107/K108, and K294/K295 (Fig. 2K). A comprehensive list of residueresidue contacts between the phosphopeptides and βarrs is provided in data S2.

The sequence analysis of M2R reveals that there are two plausible P-X-P-P–type motifs in the ICL3, one represented by T307-V-S309-T310, which is observed in the structures presented here, and the other represented by T340-N-T342-T343 (Fig. 2L). To validate the contribution of the T-V-S-T stretch in M2R-ICL3 in βarr engagement and activation, we generated two different mutants of the receptor with the phosphorylation sites in each of these P-X-P-P motifs changed to Ala residues by site-directed mutagenesis. Subsequently, we measured agonist-induced βarr1 recruitment to these mutants vis-à-vis the wild-type receptor using NanoBiT and coimmunoprecipitation assay. Mutation of T-V-S-T, but not T-N-T-T, nearly ablates βarr binding (Fig. 2, L and M, and fig. S12). These observations establish the key contribution of the T-V-S-T motif in M2R-ICL3 in driving βarr recruitment and underscore the shared mechanism of βarr activation by M2R and other prototypical GPCRs despite distinct receptor domains engaging βarrs.

βarr signaling complexes with atypical chemokine receptors

In contrast to prototypical GPCRs, some chemokine receptors, such as CXCR7, D6R, and a complement C5 receptor (C5aR2), lack G protein coupling but maintain robust βarr recruitment and downstream signaling (27, 35–38). These receptors, referred to as ACKRs or ACRs, are essentially intrinsically βarr-biased and represent an excellent model system to probe structural and functional diversity of βarrs. We thus attempted to reconstitute D6R-βarr complexes using coexpression of the receptor, GRK2 or GRK6, and βarr1/2, followed by in cellulo assembly of the complex through agonist stimulation and stabilization using Fab30. Although we observed clear complex formation and a typical architecture by negative staining that is reminiscent of the hanging conformation (Fig. 3, A and B), attempts to scale up the complex for cryo-EM analysis were not successful. Therefore, we focused our efforts to determine the structures of βarrs in complex with a phosphorylated peptide corresponding to the C terminus of D6R (D6Rpp) (Fig. 3D). We first confirmed that D6R-βarr interaction depends on receptor phosphorylation by truncating the C terminus of D6R harboring the phosphorylation sites, which resulted in near-complete ablation of agonistinduced βarr1 recruitment (Fig. 3C). Subsequently, we characterized D6Rpp using in vitro proteolysis and Fab30 reactivity assays (fig. S4, C to F) and further validated βarr activation by this peptide using hydrogen/deuterium exchange mass spectrometry (HDX-MS). We observed that D6Rpp binding resulted in robust activation of βarrs, as reflected by conformational changes in multiple β strands and loop regions in the N-domain (Fig. 3, E and F, and fig. S13). We also observed notable differences between the HDX-MS pattern of βarr1 versus βarr2, such as reduced solvent exposure of β strands XIV and XV in the C-domain of βarr2, which suggests isoformspecific differences between activation of βarr1 versus βarr2.

We determined the structures of βarr1 and βarr2 in complex with D6Rpp, stabilized by Fab30, at resolution of 3.4 and 3.2 Å, respectively (Figs. 1D and 3, G and H). We observed

Europe PMC Funders Author Manuscripts

Europe PMC Funders Author Manuscripts

a similar interaction interface of D6Rpp on N-domains of βarr1 and βarr2, although seven phosphates were resolved in the βarr2 structure compared to three in βarr1 (Fig. 3, G and H). However, we observed that three phosphate groups, on Ser^{348}, Ser^{350}, and Ser^{351}, were organized in a P-X-P-P pattern and were engaged in interactions with selected Lys and Arg residues in the N-domain of βarrs (Fig. 3I). As in M2R, there are two putative P-X-P-P motifs in D6Rpp, but our structural snapshots only capture βarrs associated with one of them (fig. S14). We also observed interdomain movement in D6Rpp-bound βarrs, reorientation of the key loop regions compared with the basal state, and disruption of the three-element and polar core network (Fig. 3, G and H, and figs. S11 and S24). A comprehensive list of residueresidue contacts between the phosphopeptides and βarrs are given in data S2.

We observe that the distal C terminus of βarr2 (Tyr^{391} to Lys^{408}) in the D6Rpp-bound conformation adopts an *a*-helical structure, which is positioned in the central crest of βarr2 (Fig. 4, A and B) through extensive interactions (fig. S15). This α helix in βarr2 forms a key dimerization interface for the two protomers in this structure and is arranged in an antiparallel coiled-coil fashion with contacts across the two protomers (Fig. 4C and data S3). We analyzed this α helix using molecular dynamics (MD) simulations and observed that it exhibits robust stability over a 2-μs simulation time frame (Fig. 4D). We also observed that this stretch of βarr2 C terminus has a propensity to adopt an α-helical conformation even in isolated form, meaning, without the βarr2 core being present. We did not observe this *a*-helical structure in D6Rpp-bound βarr1, although the corresponding segment is not resolved in the structure.

Resolution of an extended βarr C-terminal tail

Previous structures of activated βarrs, either in complex with phosphopeptides or full-length receptors, have used either truncated βarrs or the C terminus is not resolved structurally. Even in the crystal structure of βarr2 in its basal conformation, only part of the C terminus is structurally resolved (39, 40). We determined the cryo-EM structure of wildtype, full-length βarr2 and resolved a longer stretch of the C terminus (Fig. 4, F and G, and fig. S16). A stretch of the βarr2 C terminus adopts a β strand in its basal conformation and docks to the N-domain to maintain the βarr in an inactive conformation. A previous structure of the β-appendage domain of adaptin (AP2) in complex with a peptide corresponding to the C terminus of βarr1 also exhibits an *a*-helical conformation of the peptide that is positioned onto a groove in the platform sub-domain of the β-appendage (Fig. 4E) (41). The propensity of the C terminus in βarr1 and βarr2 to adopt an α-helical conformation should be explored further.

Discussion

A cryo-EM structure of a chimeric M2R with engineered vasopressin receptor 2 C terminus (M2-V2R) with βarr1 has been determined previously (11); however, the ICL3 of M2R was not resolved in the structure. It thus has not been known how M2R or other similar GPCRs with a short C terminus but relatively longer ICL3 engage βarrs (42). Our structures of M2R-βarr1 and M2Rpp-βarr2 underscore that the key interaction interface and the activation mechanism remains conserved despite distinct domains on the receptor being

Europe PMC Funders Author Manuscripts

Europe PMC Funders Author Manuscripts

used to engage βarrs. Our work reveals how two βarr isoforms are able to interact with and regulate a broad set of receptors with a structurally conserved interface and activation mechanism. Comparing βarr structures determined thus far, including the C3aRpp-βarr1 structure presented here, a higher interdomain rotation is observed in βarr2 than in βarr1 (fig. S17). We speculate that this observation may provide a mechanism for how class B GPCRs, which have a relatively stable βarr interaction, exhibit apparently higher affinity for βarr2 over βarr1 (43). A comparison of our M2R-bound βarr1 structure with a previously reported M2R-V2R-βarr1 complex reveals the hanging conformation of βarr1 with respect to the receptor (fig. S18). This observation further underlines the occurrence of the hanging conformation as a major population in the context of native M2R-βarr interaction and offers a structural framework to design guided experiments to probe functional outcomes in future studies. However, the active conformations of βarr1 were similar in terms of the interacting residues on N-domain, key loops, and C-domain rotation values (fig. S19). We observe that M2R-βarr complexes can also form engagements that resemble fully engaged conformations of GPCR-βarr complexes, as is apparent in cryo-EM and negative-staining data and more pronounced after cross-linking. Thus, it is conceivable, although not yet established, that βarr-mediated M2R internalization and desensitization follows the same paradigm as other GPCRs, with the hanging conformation being sufficient to drive endocytosis and signaling, whereas the closely engaged conformation is required for desensitization.

The observation of an α-helical conformation in βarr2 upon activation by D6Rpp is intriguing from multiple perspectives. The same conformation is not observed in βarr1, and, although this may simply be due to higher flexibility of the C terminus in βarr1, it would be anticipated that extensive interactions would allow structural visualization of the α helix if it was being formed. D6Rpp-bound βarr2 exhibits a dimeric assembly that is different from the previously determined active-like structures, such as those bound to V2Rpp, C5aR1pp, M2Rpp, and IP6 captured in a trimeric state (fig. S20 and data S3). In addition, the α helix observed in the C terminus of βarr2 in D6Rpp-bound state is also absent from the previously determined βarr2 structures. Although it cannot be completely ruled out that these differences may arise from a preferential orientation of the samples on cryo-EM grids, we speculate that these differences underscore the conformational signatures in βarrs upon interaction with GPCRs as compared with ACRs, which should be investigated further. The α helix in D6Rpp-βarr2 also suggests a “chameleon” nature of the distal C terminus to adopt a β strand in the basal state while transitioning to an α helix upon activation (Fig. 4H). Such secondary structure switching is also observed for several other proteins that exhibit functional diversity (44). The positioning of the α helix in the central crest of βarr2 may interfere with the core interaction of βarr2 with the receptor, although it remains to be experimentally visualized. This idea is supported by the overlay of D6Rpp-bound βarr2 with previously determined GPCR-βarr structures where either of the ICLs of the receptors appears to clash with the α helix in βarr2 (Fig. 4I and fig. S21). Previous studies have demonstrated the dynamic nature of βarrs and conformational space that they explore upon activation by distinct phosphorylation patterns, which are linked to distinct scaffolding outcomes and downstream functions (45–48).

There are several key questions that remain to be answered in the context of GPCR-βarr interaction. Several prototypical GPCRs are likely to engage βarrs through their ICL3 but

Europe PMC Funders Author Manuscripts

Europe PMC Funders Author Manuscripts

lack the P-X-P-P motif, and some of the ACRs, such as CXCR7 and C5aR2, lack this motif in their C terminus, but they still recruit βarrs. The structural snapshots presented here involve isolated phosphopeptides with defined phosphorylation patterns without the transmembrane core of the receptors. The receptor core imparts additional conformational changes in βarrs (49, 50), and it is likely that additional mechanisms and/or conformations of βarrs are induced by receptors, especially in terms of the positioning of the proximal region of the phosphorylated segment. However, the conserved principle of "P-X-P-P key" to open the "K-K-R-K-R-K lock" is likely to be maintained and guide βarr activation even in the context of full receptors (fig. S22). Previous studies have demonstrated that different GRKs may phosphorylate distinct residues in GPCRs, resulting in a phosphorylation barcode that may impart distinct βarr conformations and functional outcomes (51–53). Precise mapping of the phosphorylation patterns of the receptors used here by different GRKs and visualizing the resulting βarr conformations is necessary. Like GPCRs, βarrs are conformationally dynamic proteins, and it is plausible that they may explore multiple active conformations depending on the phosphorylation patterns. Stabilizing chaperones such as Fab30 may preferentially recognize some of these conformations better than the others. βarrs have a strong tendency to form various oligomeric states including dimers, trimers, tetramers, and even higher-order oligomers (54, 55), although previous structures of βarr2 either bound to IP6 (56) or GPCR phosphopeptides have revealed trimers (17). Future work should explore whether the dimeric arrangement observed here is specific to D6R. We predominantly observed dimeric arrangement in negative staining carried out at low protein concentrations that are easily achievable in a cellular context, although trimeric classes were also present.

Supplementary Material

Refer to Web version on PubMed Central for supplementary material.

Acknowledgments

We thank M. Ganguly for assistance with structural analysis and S. Mishra, A. Dalal, and N. Zaidi for help with functional assays. Cryo-EM on basal state βarr2, C3aRpp-βarr1, and D6Rpp-βarr complexes was performed at the BioEM lab of the Biozentrum at the University of Basel, and we thank C. Alampi and D. Kalbermatter for their excellent technical assistance.

Funding

Research in A.K.S.'s laboratory is supported by the Senior Fellowship of the DBT Wellcome Trust India Alliance (IA/S/20/1/504916) awarded to A.K.S., the Science and Engineering Research Board (CRG/2022/002646, SPR/2020/000408, and IPA/2020/000405), the Council of Scientific and Industrial Research [37(1730)/19/EMR-II], the Indian Council of Medical research (F.NO.52/15/2020/BIO/BMS), a Young Scientist Award from Lady Tata Memorial Trust, and IIT Kanpur. A.K.S. is an EMBO Young Investigator and Sonu Agrawal Memorial Chair Professor. This work was supported by grants from the JSPS KAKENHI, grant numbers 21H05037 (O.N.), 22K19371 and 22H02751 (W.S.), and 23KJ0491 (F.K.S.); the Kao Foundation for Arts and Sciences (W.S.); the Takeda Science Foundation (W.S.); the Lotte Foundation (W.S.); and the Platform Project for Supporting Drug Discovery and Life Science Research [Basis for Supporting Innovative Drug Discovery and Life Science Research (BINDS)] from the Japan Agency for Medical Research and Development (AMED), grant numbers JP22ama121012 (O.N.) and JP22ama121002 (support number 3272; O.N.). HDX-MS work in K.Y.C.'s laboratory was supported by grants from the National Research Foundation of Korea funded by the Korean government (NRF-2021R1A2C3003518 and NRF-2019R1A5A2027340). T.M.S. acknowledges support from the National Center of Science, Poland (2017/27/N/NZ2/02571) and Sara Borrell grant CD22/00007 funded by the Institute of Health Carlos III (ISCIII). J.S. acknowledges funding from the Instituto de Salud Carlos III (ISCIII) (AC18/00030)

and the resources of grant 2021 SGR 00046 funded by Agència de Gestió d'Ajuts Universitaris i de Recerca Generalitat de Catalunya (AGAUR).

Data and materials availability

The cryo-EM structures are deposited in Protein Data Bank (PDB) and Electron Microscopy Data Bank (EMDB) under the following accession numbers: Basal βarr2, PDB ID 8J9K and EMDB ID EMD-36110; M2R-βarr1-Fab30$^{cross\text{-}linked}$, PDB ID 8J97 and EMDB IDs EMD-36090 and EMD-36091; M2R-βarr1-Fab30, PDB ID 8JAF and EMDB IDs EMD-36126 and EMD-36093; M2Rpp-βarr2-Fab30, PDB ID 8J8R and EMDB ID EMD-36078; C3aRpp-βarr1-Fab30, PDB ID 8JA3 and EMDB ID EMD-36124; D6Rpp-βarr1-Fab30, PDB ID 8J8Z and EMDB ID EMD-36082; D6Rpp-βarr2-Fab30, PDB ID 8GO9 and EMDB ID EMD-34174; and D6Rpp-βarr2-Fab30-local-refined, PDB ID 8J8V and EMDB ID EMD-36081. All the other data pertaining to the manuscript are present in the main text and supplemental materials.

References

1. Kang DS, Tian X, Benovic JL. Curr Opin Cell Biol. 2014; 27: 63–71. [PubMed: 24680432]
2. Gurevich VV, Gurevich EV. Mol Cell Endocrinol. 2019; 484: 34–41. [PubMed: 30703488]
3. Ahn S, Shenoy SK, Luttrell LM, Lefkowitz RJ. Cell. 2020; 182: 1362–1362.e1. [PubMed: 32888497]
4. Maharana J, Banerjee R, Yadav MK, Sarma P, Shukla AK. Curr Opin Struct Biol. 2022; 75 102406 [PubMed: 35738165]
5. Ranjan R, Dwivedi H, Baidya M, Kumar M, Shukla AK. Trends Cell Biol. 2017; 27: 851–862. [PubMed: 28651823]
6. Grimes J, et al. Cell. 2023; 186: 2238–2255. e20 [PubMed: 37146613]
7. Janetzko J, et al. Cell. 2022; 185: 4560–4573. e19 [PubMed: 36368322]
8. Eichel K, Jullié M, et al. Nature. 2018; 557: 381–386. [PubMed: 29720660]
9. Eichel K, von Zastrow M. Nat Cell Biol. 2016; 18: 303–310. [PubMed: 26829388]
10. Ranjan R, Gupta P, Shukla AK. Curr Biol. 2016; 26: R285–R288. [PubMed: 27046816]
11. Staus DP, et al. Nature. 2020; 579: 297–302. [PubMed: 31945772]
12. Huang W, et al. Nature. 2020; 579: 303–308. [PubMed: 31945771]
13. Lee Y, et al. Nature. 2020; 583: 862–866. [PubMed: 32555462]
14. Cao C, et al. Neuron. 2022; 110: 3154–3167. e7 [PubMed: 36087581]
15. Yin W, et al. Cell Res. 2019; 29: 971–983. [PubMed: 31776446]
16. Bous J, et al. Sci Adv. 2022; 8 eabo7761 [PubMed: 36054364]
17. Maharana J, et al. Mol Cell. 2023; 83: 2091–2107. e7 [PubMed: 37209686]
18. Isaikina P, et al. Mol Cell. 2023; 83: 2108–2121. e7 [PubMed: 37244255]
19. Mayer D, et al. Nat Commun. 2019; 10 1261 [PubMed: 30890705]
20. Zhou XE, et al. Cell. 2017; 170: 457–469. e13 [PubMed: 28753425]
21. Tobin AB, Butcher AJ, Kong KC. Trends Pharmacol Sci. 2008; 29: 413–420. [PubMed: 18606460]
22. Tobin AB. Br J Pharmacol. 2008; 153 (suppl. 1) S167–S176. [PubMed: 18193069]
23. DeGraff JL, Gurevich VV, Benovic JL. J Biol Chem. 2002; 277: 43247–43252. [PubMed: 12205092]
24. Pals-Rylaarsdam R, et al. J Biol Chem. 1997; 272: 23682–23689. [PubMed: 9295310]
25. Hosey MM, et al. Life Sci. 1999; 64: 363–368. [PubMed: 10069497]
26. Pandey S, Maharana J, Li XX, Woodruff TM, Shukla AK. Trends Biochem Sci. 2020; 45: 693–705. [PubMed: 32402749]
27. Pandey S, et al. Mol Cell. 2021; 81: 4605–4621. e11 [PubMed: 34582793]

Europe PMC Funders Author Manuscripts
Europe PMC Funders Author Manuscripts

Europe PMC Funders Author Manuscripts

28. Rajagopal S, et al. βProc Natl Acad Sci USA. 2010; 107: 628–632. [PubMed: 20018651]
29. Borroni EM, et al. Sci Signal. 2013; 6 ra30
30. Ulvmar MH, Hub E, Rot A. Exp Cell Res. 2011; 317: 556–568. [PubMed: 21272574]
31. Graham GJ, Locati M, Mantovani A, Rot A, Thelen M. Immunol Lett. 2012; 145: 30–38. [PubMed: 22698181]
32. Cancellieri C, Vacchini A, Locati M, Bonecchi R, Borroni EM. Biochem Soc Trans. 2013; 41: 231–236. [PubMed: 23356288]
33. Nibbs RJ, Graham GJ. Nat Rev Immunol. 2013; 13: 815–829. [PubMed: 24319779]
34. Shukla AK, et al. Nature. 2014; 512: 218–222. [PubMed: 25043026]
35. Pandey S, et al. J Biol Chem. 2019; 294: 9416–9429. [PubMed: 31036565]
36. Croker DE, et al. Immunol Cell Biol. 2016; 94: 787–795. [PubMed: 27108698]
37. Yen YC, et al. Sci Adv. 2022; 8 eabn8063 [PubMed: 35857509]
38. Nguyen HT, et al. Cell Biosci. 2020; 10: 134. [PubMed: 33292475]
39. Han M, Gurevich VV, Vishnivetskiy SA, Sigler PB, Schubert C. Structure. 2001; 9: 869–880. [PubMed: 11566136]
40. Zhan X, Gimenez LE, Gurevich VV, Spiller BW. J Mol Biol. 2011; 406: 467–478. [PubMed: 21215759]
41. Schmid EM, et al. PLOS Biol. 2006; 4: e262. [PubMed: 16903783]
42. Seyedabadi M, Gharghabi M, Gurevich EV, Gurevich VV. Biomolecules. 2021; 11: 218. [PubMed: 33557162]
43. Oakley RH, Laporte SA, Holt JA, Caron MG, Barak LS. J Biol Chem. 2000; 275: 17201–17210. [PubMed: 10748214]
44. Porter LL, et al. Nat Commun. 2022; 13 3802 [PubMed: 35778397]
45. Liu Q, et al. Nat Commun. 2020; 11 4857 [PubMed: 32978402]
46. He QT, et al. Nat Commun. 2021; 12 2396 [PubMed: 33888704]
47. Coffa S, Breitman M, Spiller BW, Gurevich VV. Biochemistry. 2011; 50: 6951–6958. [PubMed: 21732673]
48. Peterson YK, Luttrell LM. Pharmacol Rev. 2017; 69: 256–297. [PubMed: 28626043]
49. Ghosh E, et al. Cell Rep. 2019; 28: 3287–3299. e6 [PubMed: 31553900]
50. Latorraca NR, et al. Nature. 2018; 557: 452–456. [PubMed: 29720655]
51. Nobles KN, et al. Sci Signal. 2011; 4 ra51 [PubMed: 21868357]
52. Reiter E, Ahn S, Shukla AK, Lefkowitz RJ. Annu Rev Pharmacol Toxicol. 2012; 52: 179–197. [PubMed: 21942629]
53. Shukla AK, et al. Proc Natl Acad Sci USA. 2008; 105: 9988–9993. [PubMed: 18621717]
54. Chen Q, et al. J Mol Biol. 2021; 433 166790 [PubMed: 33387531]
55. Gurevich VV, Gurevich EV. Int J Mol Sci. 2022; 23 7253 [PubMed: 35806256]
56. Chen Q, et al. Nat Commun. 2017; 8: 1427. [PubMed: 29127291]

Europe PMC Funders Author Manuscripts

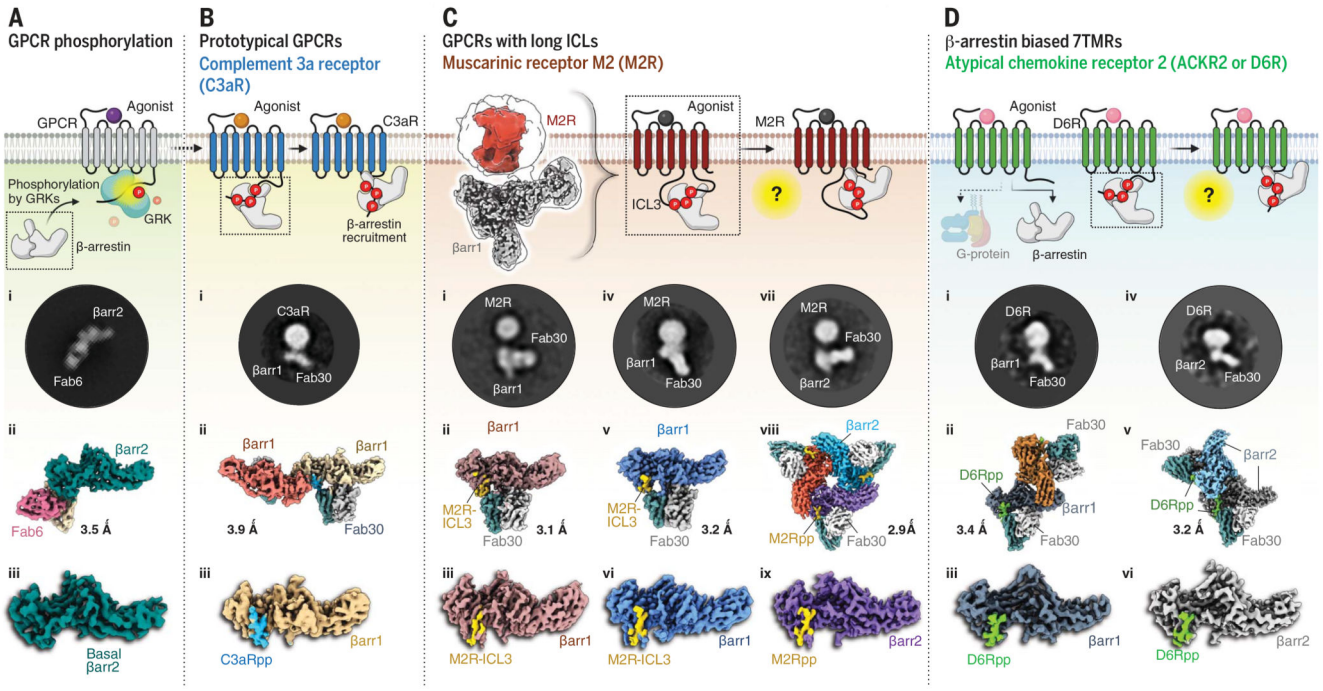

Fig. 1. A structural approach to understand the atypical modes of βarr interaction with 7TMRs.

(A) Cryo-EM structure of full-length βarr2 sheds light on its basal-state conformation. 2D class average (i), overall 3D map of βarr2 bound to Fab6 (ii), and structure of βarr2 alone (iii). **(B)** b-arrestins adopt two distinct modes of interaction with phosphorylated typical GPCRs. The phosphorylation pattern of complement receptor C3aR was used to delineate the "hanging" mode of βarr interaction. 2D class average (i), overall dimeric 3D map (ii), and structure of C3aRpp-βarr1 (iii). **(C)** A 3D reconstruction (left) showing a "hanging" mode of complex organization in M2R. High-resolution structures of M2R-ICL3–bound βarr1/2 are shown below. 2D class average (i), overall 3D map (ii), and structure of M2R-βarr1 (iii); M2R-βarr1 of cross-linked complex (iv, v, and vi); and M2Rpp-βarr2 (vii, viii, and ix). **(D)** 2D class average (i), overall dimeric 3D map (ii), and structure (iii) of D6Rpp-βarr1, and D6Rpp-βarr2 (iv, v, and vi). The estimated resolutions for all the structures are shown next to each map.

Europe PMC Funders Author Manuscripts
Europe PMC Funders Author Manuscripts

Europe PMC Funders Author Manuscripts

Europe PMC Funders Author Manuscripts

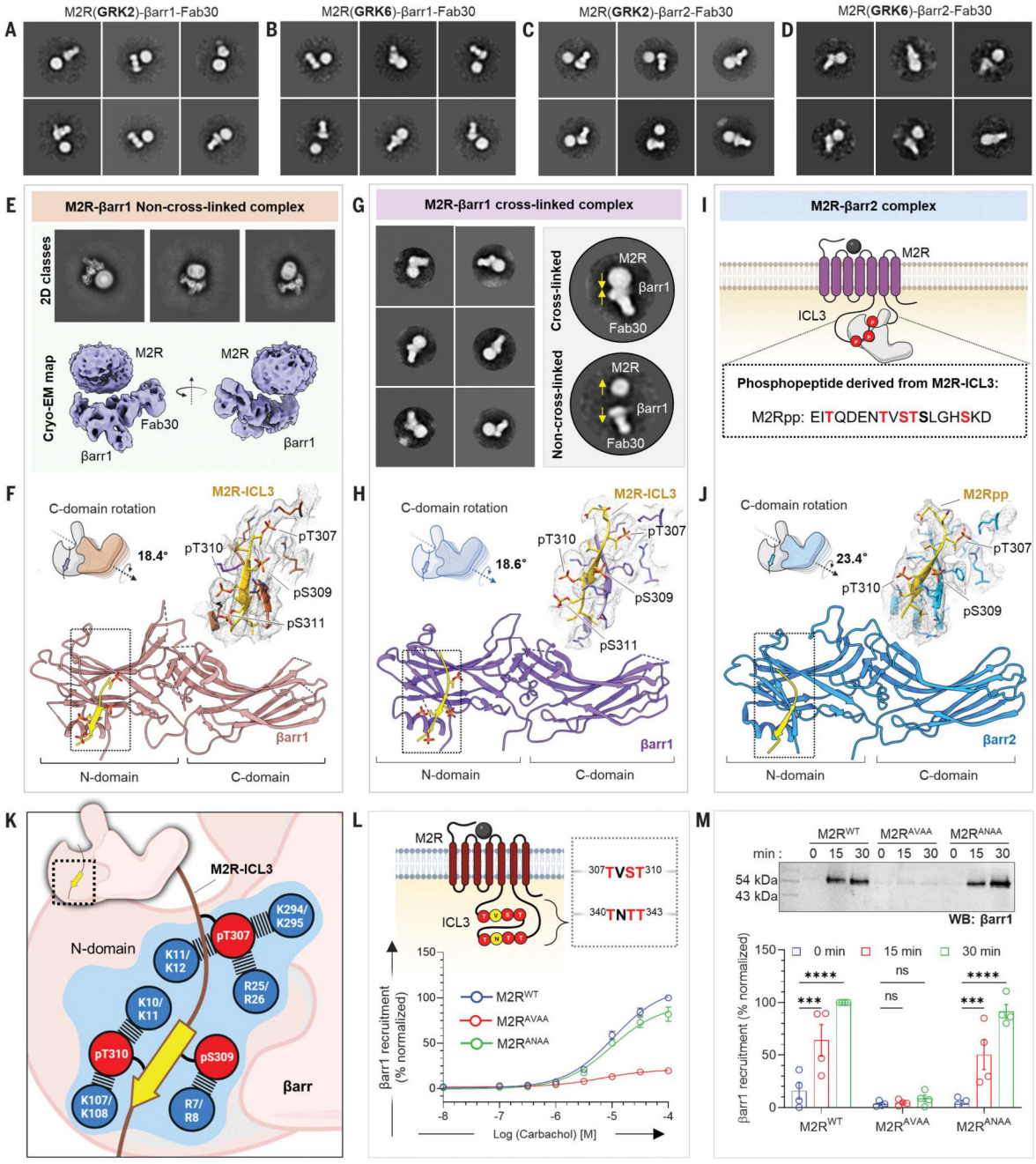

Fig. 2. Structural insights into ICL3-driven βarr interaction with M2R.

(**A** to **D**) Negative-staining EM class averages of M2R, endogenously phosphorylated by GRK2/6 in complex with βarr1 or βarr2. (**E**) Cryo-EM 2D classes, 3D reconstruction of "hanging" M2R-βarr1-Fab30 complex. (**F**) Structure of βarr1 bound to phosphorylated M2R-ICL3. The EM density of ICL3 and surrounding residues within 4 Å are shown in the inset. βarr1 attains an active conformation with a C-domain rotation of 18.4° with respect to the N-domain. (**G**) Representative negative-staining EM 2D classes depicting the effect of cross-linking. Yellow arrows show potential transition of the complex subunits.

(**H**) Structure of the crosslinked M2R-βarr1 complex. The EM density of ICL3 and surrounding residues within 4 Å are shown in the inset. C-domain rotation value with respect to N-domain is 18.6°. (**I**) Sequence of phosphopeptide derived from the ICL3 of M2R. (**J**) Structure of M2Rpp-βarr2 in ribbon representation. M2Rpp is shown in yellow and βarr2 in blue. Density map of phosphopeptide and surrounding residues within 4Å are displayed to the right. βarr2 attains an active conformation with 23.4° rotation of C-domain upon activation with M2Rpp. (**K**) The phosphorylated residues from ICL3 making critical contacts with Lys and Arg residues of βarr1 (upper) and βarr2 (lower) are highlighted in blue. (**L**) Cartoon representation illustrating the presence of possible phosphorylation clusters in the ICL3 of M2R. Mutations of the two phosphor-motifs: TVST and TNTT were generated to assess the βarr recruitment measured by bystander NanoBiT assay (receptor+SmBiT-βarr1+LgBiT-CAAX). Substitution of phosphosites of TVST to AVAA leads to abrupt reduction in βarr recruitment, whereas TNTT to ANAA substitution maintains βarr recruitment, suggesting a critical role played by TVST on βarr recruitment to M2R (mean ± SEM; n = 3 independent experiments; normalized with respect to highest ligand concentration signal for M2RWT as 100%). (**M**) Role of TVST in βarr recruitment is further corroborated by coimmunoprecipitation assay. On carbachol stimulation, $M2R_{AVAA}$ showed drastic reduction in βarr1 recruitment. A representative blot and densitometry-based quantification are presented (mean ± SEM; n = 4 independent experiments; normalized with M2R 30-min stimulation condition signal as 100%; two-way analysis of variance, Tukey's multiple comparisons test). The exact P values are as follows: $M2R_{WT}$ 0 min versus 15 min, P = 0.0006;$M2R_{WT}$ 0 min versus 30 min, P = <0.0001; $M2R_{ANAA}$ 0 min versus 15 min, P = 0.0008;$M2R_{ANAA}$ 0 min versus 30 min, P = <0.0001 (***P = 0.0001; ****P < 0.0001; ns, nonsignificant). Single-letter abbreviations for the amino acid residues are as follows: A, Ala; C, Cys; D, Asp; E, Glu; F, Phe; G, Gly; H, His; I, Ile; K, Lys; L, Leu; M, Met; N, Asn; P, Pro; Q, Gln; R, Arg; S, Ser; T, Thr; V, Val; W, Trp; and Y, Tyr.

Europe PMC Funders Author Manuscripts

Europe PMC Funders Author Manuscripts

Europe PMC Funders Author Manuscripts

Europe PMC Funders Author Manuscripts

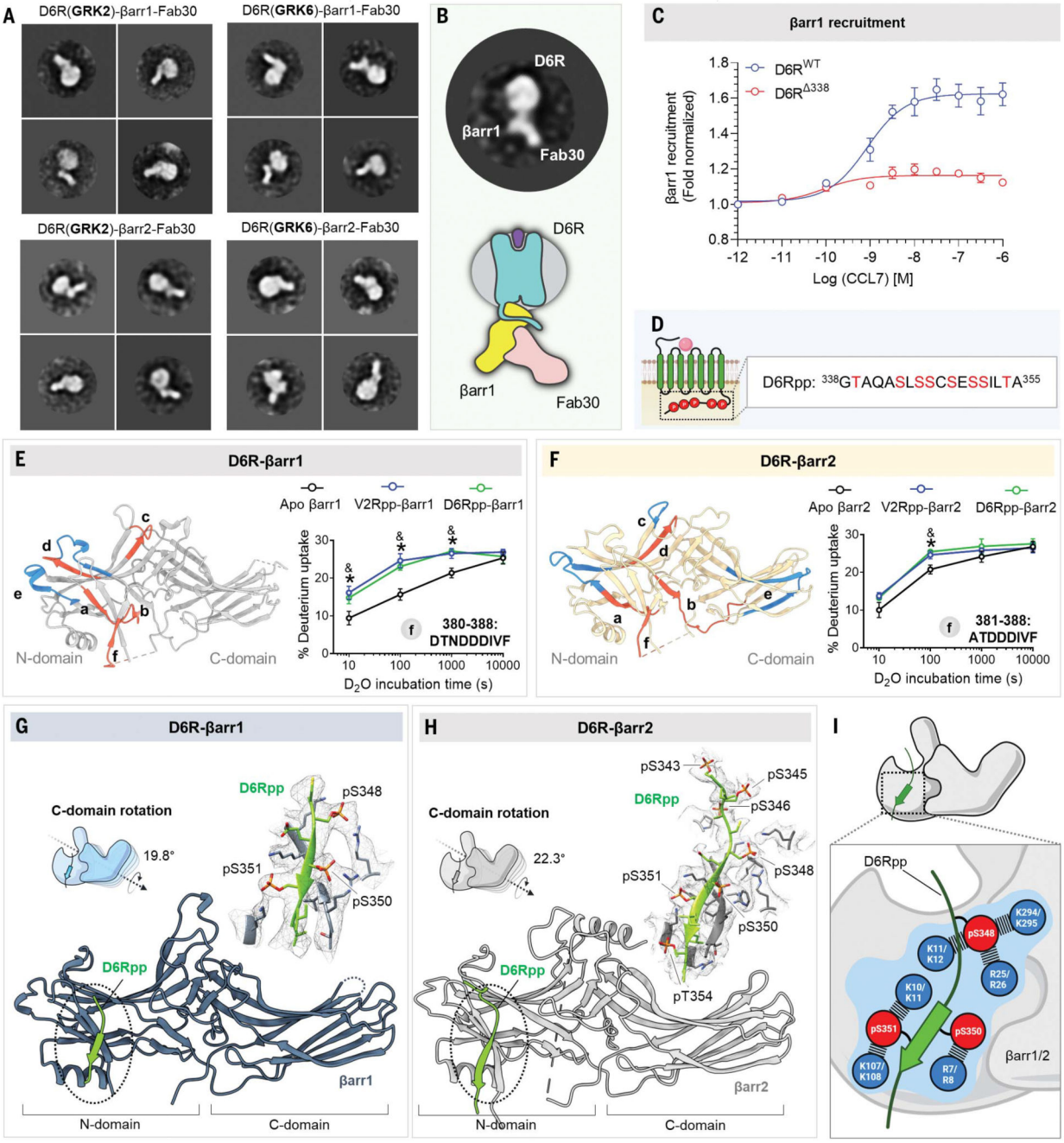

Fig. 3. Structural insights into D6R-βarr complex interaction and activation.

(A) Negative-staining EM 2D class averages of D6R-βarr1/2 complexes endogenously phosphorylated with GRK2/6. (**B**) A representative 2D class average highlighting the "hanging" mode of βarr1 interaction with the receptor. (**C)** Dose response curve for CCL7-induced βarr1 recruitment for the mentioned D6R constructs using NanoBiT assay (Receptor-SmBiT+LgBiT-βarr1) (mean ± SEM; n = 3 independent experiments; normalized with respect to the lowest ligand concentration signal as 1). (**D)** Design of selected phosphopeptide derived from the C terminus of D6R. (**E** and **F**) HDX-MS plots to show the

potential of generated phosphopeptides from D6R to activate βarr1 and βarr2, respectively. Among regions (a to f) showing significant changes upon deuterium exchange, the fragment at the C terminus (f) has been demonstrated to show activation of βarrs upon D6Rpp binding. (**G**) Structure of D6Rpp-βarr1 complex in ribbon representation. The density map of D6Rpp and surrounding residues within 4 Å are shown to the left. C-domain rotation of βarr1 bound to D6Rpp is 19.8°. (**H**) Structure of D6Rpp-βarr2 complex in ribbon representation. The density map of D6Rpp and surrounding residues within 4 Å are shown in the inset. C-domain rotation of βarr2 bound to D6Rpp was calculated to be 22.3°. (**I**) The phosphorylation pattern from D6Rpp engages with a network of Lys and Arg residues present on the N-domains of βarrs. Residues highlighted with blue circles show the Lys and Arg residues in βarr1 (upper) and βarr2 (lower).

Europe PMC Funders Author Manuscripts

Europe PMC Funders Author Manuscripts

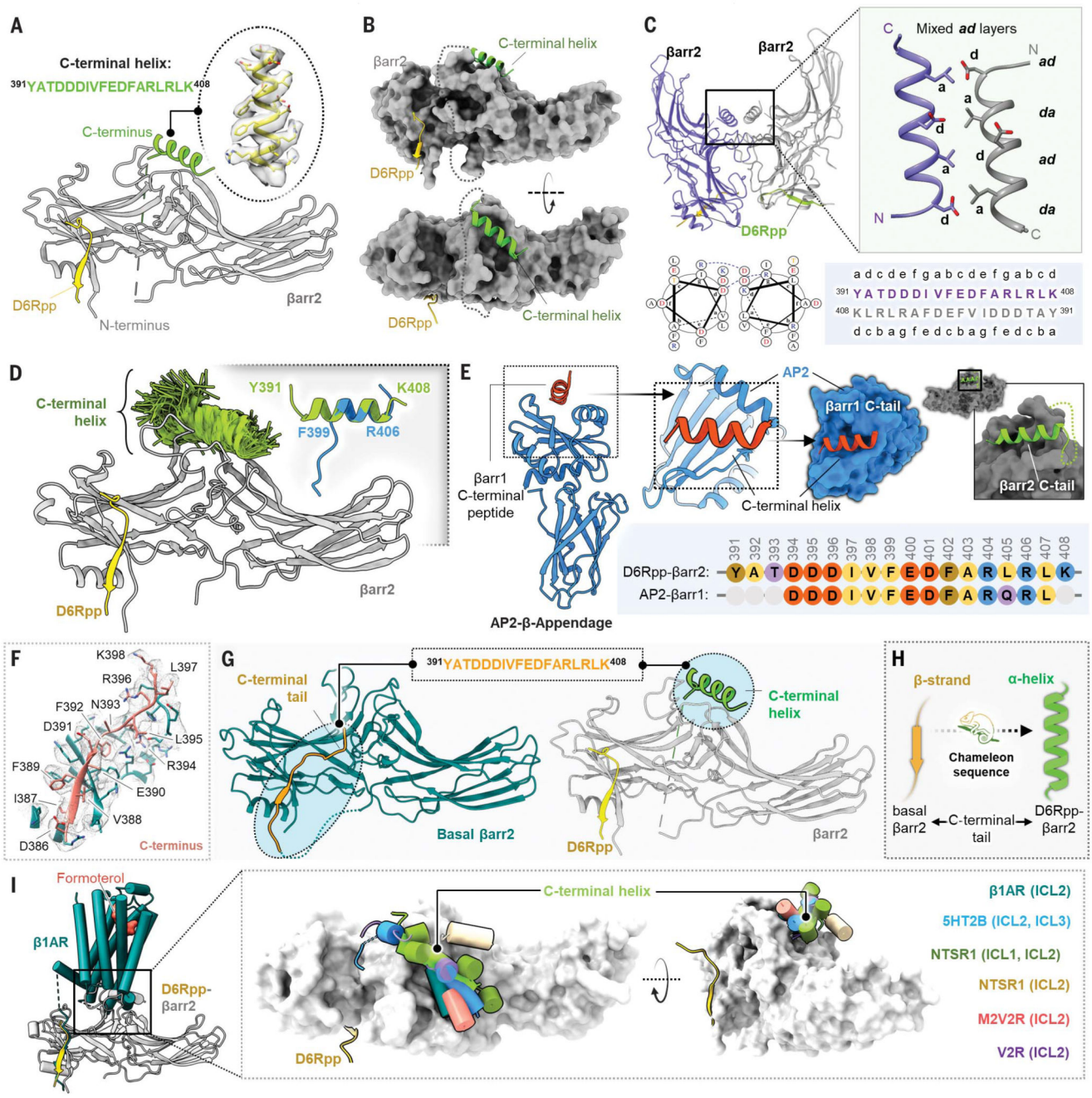

Fig. 4. Discovery of a C-terminal helix in D6R-activated βarr2.

(A) Cartoon representation of βarr2 bound to D6R phosphopeptide. βarr2 and D6Rpp are presented in gray and yellow, respectively, and the sequence of the C-terminal helix is shown in the inset. (**B**) D6Rpp-βarr2 structure displayed in surface representation in two different views to highlight the pose of the helix. The C-terminal helix (green) and D6Rpp (yellow) are shown as ribbon diagrams. (**C**) Dimeric organization of D6Rpp-βarr2 structure shown in ribbon representation (top left). Formation of antiparallel coiled-coil by the C-terminal helix of βarr2 at the dimeric interface (top right) shown as cartoon representation. The antiparallel

Europe PMC Funders Author Manuscripts
Europe PMC Funders Author Manuscripts

Europe PMC Funders Author Manuscripts

Europe PMC Funders Author Manuscripts

coiled-coil exhibits mixed *ad* layers. Helical wheel representation of the antiparallel coiled-coil shows Asp at position *d* of one helix, which forms a salt bridge with Arg at position *g* in the other helix (bottom left). Heptad helical representation of the antiparallel coiled-coil residues in the βarr2 sequence (bottom right). (**D**) MD simulations confirm stability of the distal C-terminal helix/βarr2 interface. Structural snapshots (one snapshot every 10 ns, 7 × 250 ns of simulation time) presented here are of the position of the C-tail during simulation. For each residue, frames where it assembles an α-helical conformation are colored green. Fragments of the C-terminal helix can spontaneously assemble an a-helical conformation (right corner, blue cartoon) in three out of four independent MD simulations (each 2 μs) which is overlayed with the crystallized C-tail for comparison (green cartoon). For each residue, frames where it assembles a helical conformation are colored green. Comparison of a spontaneously assembled helical conformation of the βarr2 C-tail (blue) with that present in the structure (gray). (**E)** Structure of AP2 b-appendage protein in complex with βarr1 C-terminal peptide (PDB ID 2IV8) is shown as cartoon representation (left). The βarr1 C-terminal peptide can be seen to adopt similar helical conformation as the C-terminal helix in the D6Rpp-bound βarr2 structure (right). The sequence alignment of the C-terminal stretches of βarr1 and βarr2 are shown in the inset. (**F**) Cryo-EM density map of the isolated C terminus of βarr2 and surrounding residues within 4Å. (**G**) The peptide stretch sequence (top) of the C-tail in basal βarr2 transforms into a helical conformation in the D6Rpp-bound state (highlighted in cyan circles). (**H**) The C-tail of βarr2 exhibits a chameleon-like property, adopting a helical conformation in the active state from a β strand in the basal state. **(I**) Ribbon representation of the β1AR-βarr1 structure superimposed with D6Rpp-βarr2 on βarrs (left) shows positioning of the C-terminal helix on the central crest of βarrs. Upon structural superimposition with all reported GPCR-βarr1 structures, ICL1/2/3 of various receptors reside on the central crest as a C-terminal helix on D6Rpp-βarr2 (right).